Anharmonicity due to Electron-Phonon Coupling in Magnetite

Moritz Hoesch,[1] Przemysław Piekarz,[2] Alexey Bosak,[3] Mathieu Le Tacon,[4] Michael Krisch,[3]
Andrzej Kozłowski,[5] Andrzej M. Oleś,[4,6] and Krzysztof Parlinski[2]

[1]*Diamond Light Source, Harwell Campus, Didcot OX11 0DE, Oxfordshire, United Kingdom*
[2]*Institute of Nuclear Physics, Polish Academy of Sciences, Radzikowskiego 152, PL-31342 Kraków, Poland*
[3]*European Synchrotron Radiation Facility, 6 rue Jules Horowitz, F-38043 Grenoble Cedex, France*
[4]*Max-Planck-Institut für Festkörperforschung, Heisenbergstrasse 1, D-70569 Stuttgart, Germany*
[5]*Faculty of Physics and Applied Computer Science, AGH-University of Science and Technology,
Aleja Mickiewicza 30, PL-30059 Kraków, Poland*
[6]*Marian Smoluchowski Institute of Physics, Jagellonian University, Reymonta 4, PL-30059 Kraków, Poland*
(Received 3 October 2012; published 13 May 2013)

We present the results of inelastic x-ray scattering for magnetite and analyze the energies and widths of
the phonon modes with different symmetries in a broad range of temperature $125 < T < 293$ K. The
phonon modes with X_4 and Δ_5 symmetries broaden in a nonlinear way with decreasing T when the
Verwey transition is approached. It is found that the maxima of phonon widths occur away from high-
symmetry points, which suggests the incommensurate character of critical fluctuations. Strong phonon
anharmonicity induced by electron-phonon coupling is discovered by a combination of these experimental
results with *ab initio* calculations which take into account local Coulomb interactions at Fe ions.
It (i) explains observed anomalous phonon broadening and (ii) demonstrates that the Verwey transition
is a cooperative phenomenon which involves a wide spectrum of phonons coupled to the electron charge
fluctuations condensing in the low-symmetry phase.

Discovered in ancient Greece, magnetite played a
crucial role in the history of magnetism. Apart from its
magnetic properties, which found numerous technological
applications during the past century, magnetite exhibits
extraordinary behavior connected with the Verwey transi-
tion [1]. The most prominent feature observed upon
lowering the temperature is the discontinuous reduction
of the electric conductivity by 2 orders of magnitude at
$T_V = 122$ K. Extensive experimental and theoretical stud-
ies of magnetite during past decades revealed very com-
plex interrelations between the electronic and structural
degrees of freedom, which both participate in the Verwey
phase transition [2,3]. In spite of this progress, the transi-
tion is not yet fully understood and remains a very intrigu-
ing phenomenon in condensed matter physics.

At the Verwey transition, the crystal structure changes
from the high-temperature cubic $Fd\bar{3}m$ to the low-
temperature monoclinic Cc symmetry [4]. It was first
believed that octahedral B sites, with mixed-valence
$Fe^{2.5+}$ ions turn to distinct Fe^{2+} and Fe^{3+} ions below T_V.
Detailed diffraction studies of the low-temperature phase
revealed a much more complex charge-order pattern [5],
with a wide distribution of valences at the octahedral sites
[6], and an orbitally ordered pattern distributed over three
Fe sites (trimerons) [7]. These observations are consistent
with *ab initio* calculations [8,9] and resonant x-ray scat-
tering studies [10–13], that additionally suggest the charge-
orbital (CO) order appearing a few kelvins above T_V [14]
and possibly existing in the dynamic form even at higher

temperatures [15]. Since the existence of CO order above
the Verwey transition has been questioned by other studies
[16] and its role in this transition is under debate at present
[13], experiments performed above T_V might resolve this
controversy.

The key element, which stabilizes the CO order and
drives the crystal symmetry change, is the coupling between
electronic and vibrational degrees of freedom. Such coop-
erative nature of the Verwey transition is supported by
numerous experimental observations: oxygen isotope effect
[17], critical softening of the c_{44} elastic constant [18],
critical diffuse scattering [19,20], and phonon anomalies
measured by Brillouin [21], Raman [22], and nuclear in-
elastic scattering [23,24]. The instability of the electronic
structure is intimately connected with a lattice deformation,
with certain similarity to the Peierls model [25]. In the
simplest model, one can explain the doubling of the unit
cell along the c direction by the condensation of the acoustic
Δ_5 mode at $\vec{q} = (0, 0, 1/2)$ [26], whereas the monoclinic
distortion requires at least two primary order parameters
with Δ_5 and X_3 symmetries [27].

In this Letter, we report a lattice dynamics study of
magnetite over a wide range of temperatures above T_V
and address the question of whether or not the electron-
phonon coupling in the presence of CO fluctuations is the
principal cause of the Verwey transition. Our study reveals
increasing anomalous broadening of the lowest transverse
acoustic (TA) modes along the [001] (Δ) and transverse
optic (TO) modes along the [110] (Σ) directions as

temperature decreases towards T_V. We show by density functional theory calculations that the anharmonic phonon behavior discovered here (i) is a direct consequence of the electron-phonon coupling and (ii) occurs only in the presence of strong electronic correlations, which is a novel aspect of the Verwey transition.

Momentum resolved vibrational spectra were obtained by inelastic x-ray scattering (IXS) at beam line ID28 at the European Synchrotron Radiation Facility (ESRF) [28]. Two settings with energy resolution of $\delta E = 1.6$ and 3.2 meV were used. The sample was a single crystal of magnetite, skull melter grown at Purdue University and annealed for stoichiometry [29]. The sample temperature was measured using a Si diode sensor on the copper cold finger of the closed cycle cryostat.

The momentum points Q to be measured were chosen from the calculations presented below. From the calculated phonon eigenvectors the IXS intensity was predicted and favorable X points Q were selected from the highest contrast against other modes and high total intensity. The most suitable X_4 mode was found at $Q = (554)$. The optimal X_3 mode was found at $Q = (445)$ with a slight contribution from the X_4 mode in the spectra. The lowest optical Δ_5 mode was measured along the line from $Q = (333)$ to $Q = (334)$.

Raw data with $\delta E = 1.6$ meV at the Brillouin zone boundary point X are shown in Fig. 1. The lowest energy X_4 phonon displays a significant broadening, while the lowest X_3 phonon is only slightly broader than the experimental resolution. As the temperature is lowered towards T_V the diffuse scattering intensity at zero energy loss strongly increases. The phonon energies, on the other hand, show no readily visible temperature dependence.
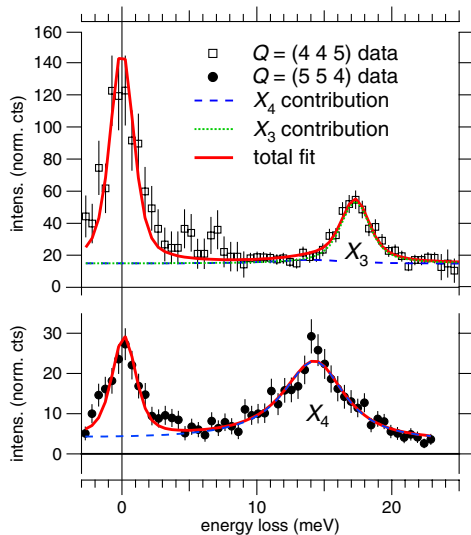
To extract precise phonon energies and peak widths the spectra were numerically fitted by a superposition of peaks derived from the measured resolution function. For visibly enlarged phonon peaks these were convoluted with a Lorentzian function. For the quasielastic intensity no convolution was applied. The spectra at (554) of Fig. 1 were thus analyzed first, and the determined phonon energy and width were kept fixed for the fit of the data at (445). The free parameters were the intensities and one phonon energy and width per spectrum. We found that the broadening had to be applied to the X_4 mode and all connected branches, while the X_3 mode and connected branches remained close to resolution limited.

The thus determined phonon dispersions from data at $\delta E = 3.2$ meV are shown in Figs. 2(a) and 2(b) for branches connected to X_4 and in Fig. 3 for X_3. Figure 3 also includes room temperature inelastic neutron scattering data [30] and the acoustic Σ_3-TA mode is fit by a model sinusoidal dispersion, which reveals a downward bending of the dispersion by less than 1 meV about halfway between K and Γ. The dispersions match within the error bars at both room temperature and $T = 129$ K, with only a slight hardening at low temperature visible for the X_4 mode, in agreement with the measured Fe density of states [23,24] (below T_V the multitwinned nature of the sample prevents the determination of the phonon dispersion). In the following the Δ_5-TA, Σ_1-TO, and Σ_2-TO will be denoted as the branches connected to X_4, and Δ_5-TO and Σ_3-TA as connected to X_3. In contrast, the phonon widths in Figs. 2(c) and 2(d) have a much stronger temperature dependence. The width increases on lowering the

FIG. 1 (color online).   Inelastic x-ray scattering spectra of Fe_3O_4 at $T = 150$ K. The intensity is shown in units of detector counts normalized to a monitor. At $Q = (554)$ scattering from the X_4 phonon and at $Q = (445)$ from the X_3 phonon with a small contribution from X_4 are dominant. The energy resolution is 1.6 meV.
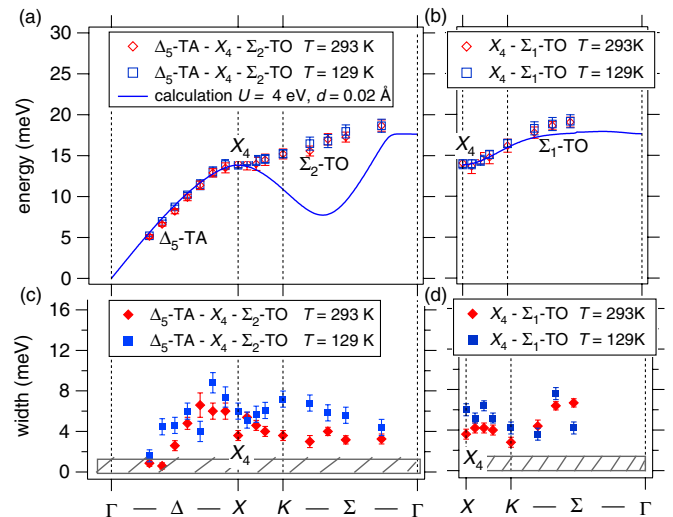

FIG. 2 (color online).   (a, b) Phonon energies determined by peak fitting as a function of reduced wave vector for branches connected to X_4, measured in the vicinity of (554), for $T = 293$ K and $T = 129$ K. Calculated phonon dispersions are plotted with solid lines. (c), (d) Phonon widths of branches connected to X_4 as a function of reduced wave vector.
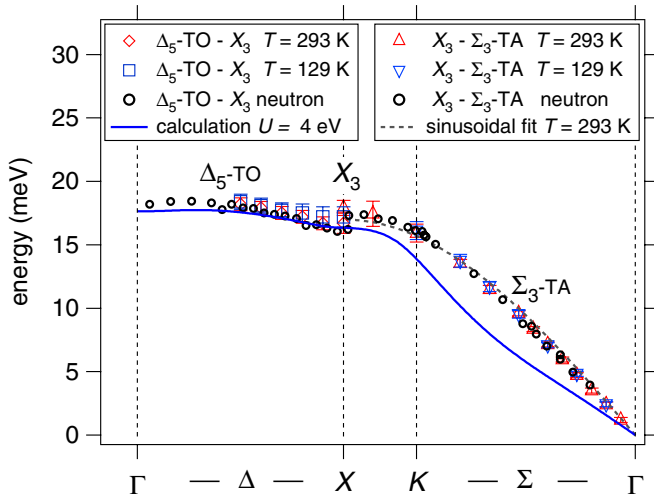
FIG. 3 (color online).   Phonon energies as a function of reduced wave vector for branches connected to X_3, measured in the vicinity of (445) and (334). Data at two temperatures $T = 293$ K and $T = 129$ K are shown. Calculated phonon dispersions are plotted with solid lines. Data from neutron scattering at room temperature [30] and a sinusoidal fit to represent a typical phonon dispersion are also shown.

temperature, which contradicts the usual situation, where anharmonicity increases with increasing temperature due to phonon-phonon interactions.

The full temperature dependence of selected modes, measured with $\delta E = 1.6$ meV, is shown in Fig. 4. Remarkably, the modes connected to X_4 show an increasing width on lowering the temperature towards T_V. The X_4 and Δ_5-TA phonons already show anomalous widths at room temperature moderately increasing with decreasing temperature. After reaching maximum values around 150 K, their widths are reduced again in a temperature range of about 20 K above T_V. The Σ_1 and Σ_2 modes, measured at the K point, show even stronger and linear increase of widths over the entire range of temperatures.

The density functional theory calculations were performed using the VASP program [31] within the generalized gradient approximation (GGA) and the full-potential projector-augmented wave method [32]. Phonon energies for the cubic $Fd\bar{3}m$ symmetry were calculated in the $1 \times 1 \times 1$ supercell with 56 atoms using the direct method [33], implemented in the PHONON program [34]. On the basis of the Hellmann-Feynman theorem, the atomic forces were obtained by displacing atoms from their equilibrium positions. For the cubic symmetry only three independent displacements of Fe(A), Fe(B), and O atoms are sufficient to derive all force-constant matrix elements and the dynamical matrix. In order to study anharmonic effects, we have calculated the Hellmann-Feynman forces and phonon energies for two independent sets of displacements with the amplitudes $u = 0.02$ and 0.04 Å. The effect of local electron interactions on phonon energies was investigated by performing calculations within the $GGA + U$
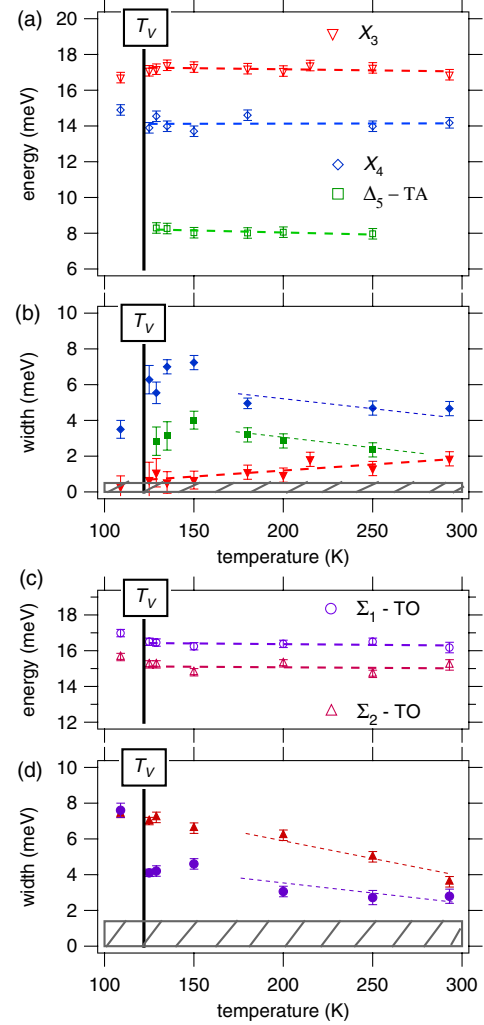

FIG. 4 (color online).   (a), (c) Energies of phonon modes as functions of temperature: (a) Δ_5, X_4, and X_3, and (c) Σ_1 and Σ_2 (at the K point). Widths of these phonon modes are displayed in (b) and (d), respectively. Straight dashed lines in (b) and (d) were fitted to points at high temperature. Widths within the hatched area are not reliably extracted from the data.

approach, where the on-site Coulomb interaction and Hund's exchange parameters, $U = 4.0$ eV and $J = 0.8$ eV, are the same as in the previous studies [27].

Considering the Δ and Σ directions, we found a very good agreement for both the Δ_5 modes between the experimental points and the calculated phonon dispersions for $u = 0.02$ Å and only a small shift of the Σ_1 mode to lower energies (Fig. 2). The largest discrepancy is found for the Σ_2 mode, which shows anomalous softening induced by the local electron interactions [27], directly connected with the anharmonic behavior discussed below. The Σ_3 mode exhibits anomalous downward bending, much larger than those observed in the experiment.

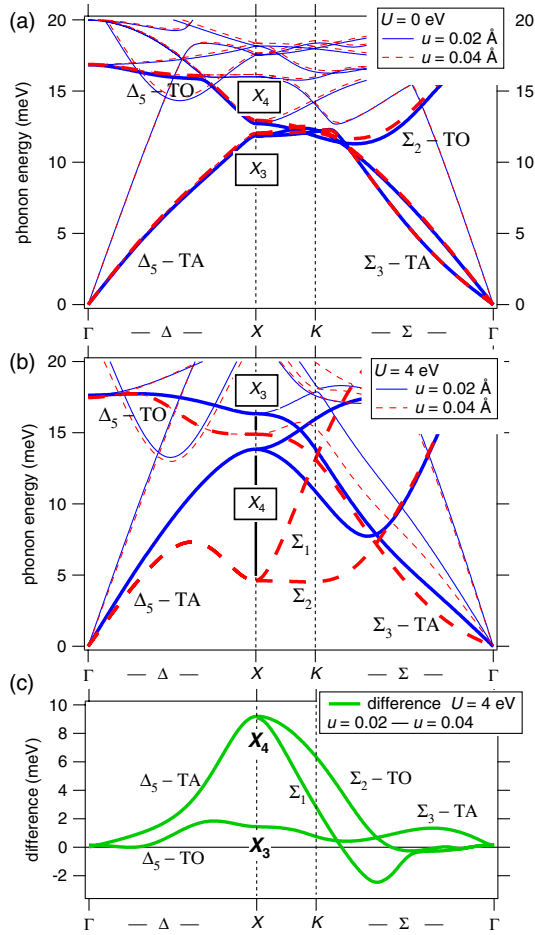Coulomb interactions strongly influence phonon dispersions. For $U = 0$ [Fig. 5(a)] the phonon energies obtained

FIG. 5 (color online). Calculated phonon dispersions of Fe_3O_4 obtained from $GGA + U$ combined with the PHONON software [34], for (a) $U = 0$ and (b) $U = 4$ eV, shown by solid (dashed) lines for a displacement of $u = 0.02$ Å (0.04 Å). Selected branches connected to the lowest X_3 and X_4 optical modes are highlighted. The difference between the phonon dispersions obtained at both values of u for $U = 4$ eV is shown in (c).

for $u = 0.02$ and 0.04 Å are very close to each other and differ by less than 0.5 meV (not shown), which means slight hardening of phonons for increasing displacement amplitudes. It demonstrates that the system is harmonic and phonon frequencies depend only very weakly on vibrational amplitudes. The situation changes in a dramatic way in the presence of local electron interactions [see Figs. 5(b) and 5(c)]—for $U = 4$ eV the phonon energies depend strongly on u and substantially soften for $u = 0.04$ Å. The largest changes are observed for the branches connected to X_4 with a broad maximum in the energy differences at the X point. A weaker but still pronounced effect is visible also for branches connected to X_3.

We emphasize that the same modes which have anomalous temperature dependence of phonon widths exhibit strong anharmonic behavior in the theory when $U=4$eV. Moreover, the phonon widths for the Δ_5-TA and Σ_2-TO

modes (Fig. 2) show similar trends as the plot of energy differences; see Fig. 5(c). In both cases the largest values are located in the vicinity of the X point. Along the Δ direction, one finds a pronounced increase of values in both figures around $\vec{q} = (0, 0, \frac{1}{2})$. The phonon widths at room temperature have a maximum around $\vec{q} = (0, 0, 0.7)$ and decrease systematically when $\vec{q}$ increases towards the X point, and further along the Σ direction. At low temperature a two-peak structure for the $\vec{q}$-dependent width is apparent: one peak at $\vec{q} \simeq (0, 0, 0.8)$ and the other one at the K point.

The observed temperature dependence of the phonon widths and the exact positions of their maxima cannot be properly described within the present calculations; see Fig. 5(c). The shift of peaks away from the X point indicates the existence of incommensurate correlations, which are missing in the supercell calculations due to the geometrical constraints.

In standard theories, large phonon widths indicate either an anharmonic behavior or strong electron-phonon coupling [35]. Our *ab initio* study demonstrates that these two effects are intimately connected in magnetite and both result from local electron interactions. These interactions induce polarization of the minority-spin partly occupied t_{2g} orbitals. In such a correlated state, the coupling between electrons and lattice enhances and stabilizes the CO order, effectively reducing the total energy [27,36]. This in turn modifies the interatomic interactions and generates the anharmonic potential. Indeed, an anharmonic double-well potential has been obtained for the Δ_5 and X_3 modes in the presence of strong electron correlations [27]. This mechanism leads to the Verwey transition with the static structural distortion and frozen CO order below T_V. In contrast, above T_V the CO degrees of freedom are dynamic and couple strongly to phonons reducing their lifetimes. Therefore, we conclude that the anharmonicity in magnetite is induced by the coupling between phonons and CO fluctuations, which leads to phonon broadening [37].

We remark that a strong electron-phonon coupling is consistent with the polaronic short-range order observed above T_V [38–40]. The anomalous phonon broadening also correlates very well with the critical diffuse scattering existing over a broad region in reciprocal space and over a broad temperature range [20]. In both cases, the strongest response is observed at incommensurate wavelengths in the reciprocal space. Charge fluctuations observed in a wider temperature range may be responsible for distinct properties of the Verwey transition in nonstoichiometric or doped magnetite [24,41,42].

In summary, we have presented the IXS measurements of the lowest phonon modes along the Δ and Σ directions in magnetite above the Verwey transition—they reveal an anomalous behavior of phonon widths that *increase* with lowering temperature. Their maxima are found away from the high-symmetry points due to the incommensurate character of critical fluctuations. Within the *ab initio* study

we have found that the same phonon modes show strong softening for larger amplitudes in the presence of local electron interactions in the Fe($3d$) states. This phonon anharmonicity is induced by the charge-orbital fluctuations above T_V—it demonstrates that the Verwey transition is triggered by a cooperative electron-phonon mechanism at large U [27].

[1] E. J. W. Verwey, Nature (London) **144,** 327 (1939).
[2] M. Imada, A. Fujimori, and Y. Tokura, Rev. Mod. Phys. **70,** 1039 (1998).
[3] F. Walz, J. Phys. Condens. Matter **14,** R285 (2002).
[4] M. Iizumi, T. F. Koetzle, G. Shirane, S. Chikazumi, M. Matsui, and S. Todo, Acta Crystallogr. Sect. B **38,** 2121 (1982).
[5] J. P. Wright, J. P. Attfield, and P. G. Radaelli, Phys. Rev. Lett. **87,** 266401 (2001); Phys. Rev. B **66,** 214422 (2002).
[6] J. Blasco, J. García, and G. Subías, Phys. Rev. B **83,** 104105 (2011).
[7] M. R. Senn, J. P. Wright, and J. P. Attfield, Nature (London) **481,** 173 (2011).
[8] I. Leonov, A. N. Yaresko, V. N. Antonov, M. A. Korotin, and V. I. Anisimov, Phys. Rev. Lett. **93,** 146404 (2004).
[9] H.-T. Jeng, G. Y. Guo, and D. J. Huang, Phys. Rev. Lett. **93,** 156403 (2004).
[10] E. Nazarenko, J. E. Lorenzo, Y. Joly, J. L. Hodeau, D. Mannix, and C. Marin, Phys. Rev. Lett. **97,** 056403 (2006).
[11] J. Schlappa et al., Phys. Rev. Lett. **100,** 026406 (2008).
[12] A. Tanaka et al., Phys. Rev. Lett. **108,** 227203 (2012).
[13] G. Subías, J. García, J. Blasco, J. Herrero-Martín, M. Concepción Sánchez, J. Orna, and L. Morellón, J. Synchrotron Radiat. **19,** 159 (2012).
[14] J. E. Lorenzo, C. Mazzoli, N. Jaouen, C. Detlefs, D. Mannix, S. Grenier, Y. Joly, and C. Marin, Phys. Rev. Lett. **101,** 226401 (2008).
[15] N. Pontius et al., Appl. Phys. Lett. **98,** 182504 (2011).
[16] J. García, G. Subías, J. Herrero-Martín, J. Blasco, V. S. Cuartero, M. C. Sánchez, C. Mazzoli, and F. Yakhou, Phys. Rev. Lett. **102,** 176405 (2009).
[17] E. I. Terukov, W. Reichelt, D. Ihle, and H. Oppermann, Phys. Status Solidi B **95,** 491 (1979).
[18] H. Schwenk, S. Bareiter, C. Hinkel, B. Lüthi, Z. Kąkol, A. Kozłowski, and J. M. Honig, Eur. Phys. J. B **13,** 491 (2000).
[19] Y. Fujii, G. Shirane, and Y. Yamada, Phys. Rev. B **11,** 2036 (1975).
[20] S. M. Shapiro, M. Iizumi, and G. Shirane, Phys. Rev. B **14,** 200 (1976).
[21] Md. Motin Seikh, C. Narayana, P. A. Metcalf, J. M. Honig, and A. K. Sood, Phys. Rev. B **71,** 174106 (2005).
[22] L. V. Gasparov, D. B. Tanner, D. B. Romero, H. Berger, G. Margaritondo, and L. Forró, Phys. Rev. B **62,** 7939 (2000).
[23] B. Handke, A. Kozłowski, K. Parlinski, J. Przewoźnik, T. Ślęzak, A. I. Chumakov, L. Niesen, Z. Kąkol, and J. Korecki, Phys. Rev. B **71,** 144301 (2005).
[24] T. Kołodziej, A. Kozłowski, P. Piekarz, W. Tabiś, Z. Kąkol, M. Zając, Z. Tarnawski, J. M. Honig, A. M. Oleś, and K. Parlinski, Phys. Rev. B **85,** 104301 (2012).
[25] V. V. Shchennikov and S. V. Ovsyannikov, J. Phys. Condens. Matter **21,** 271001 (2009).
[26] D. Ihle and B. Lorenz, Phys. Status Solidi B **96,** 659 (1979).
[27] P. Piekarz, K. Parlinski, and A. M. Oleś, Phys. Rev. Lett. **97,** 156402 (2006); Phys. Rev. B **76,** 165124 (2007).
[28] M. Krisch and F. Sette, Light Scattering in Solids: Novel Materials and Techniques, Topics in Applied Physics (Springer-Verlag, Heidelberg, 2007), pp. 317–369.
[29] H. R. Harrison and R. Aragón, Mater. Res. Bull. **13,** 1097 (1978); R. Aragón, H. R. Harrison, R. H. McCallister, and C. J. Sandberg, J. Cryst. Growth **61,** 221 (1983).
[30] E. J. Samuelsen and O. Steinsvoll, Phys. Status Solidi B **61,** 615 (1974).
[31] G. Kresse and J. Furthmüller, Comput. Mater. Sci. **6,** 15 (1996).
[32] P. E. Blöchl, Phys. Rev. B **50,** 17 953 (1994).
[33] K. Parlinski, Z.-Q. Li, and Y. Kawazoe, Phys. Rev. Lett. **78,** 4063 (1997).
[34] K. Parlinski, computer code PHONON, 2011.
[35] A. A. Abrikosov, L. P. Gor'kov, and I. Y. Dzyaloshinskii, Quantum Field Theoretical Methods in Statistical Physics (Pergamon, Oxford, 1965).
[36] H. P. Pinto and S. D. Elliott, J. Phys. Condens. Matter **18,** 10 427 (2006).
[37] Interestingly, anharmonic effects or phonon line broadening are visible for the Δ_5 phonon mode and not for the X_3 mode, which strongly couples to the t_{2g} states at the Fermi energy and opens the insulating gap [27].
[38] D. Ihle and B. Lorenz, J. Phys. C **19,** 5239 (1986).
[39] S. K. Park, T. Ishikawa, and Y. Tokura, Phys. Rev. B **58,** 3717 (1998).
[40] D. Schrupp, M. Sing, M. Tsunekawa, H. Fujiwara, S. Kasai, A. Sekiyama, S. Suga, T. Muro, V. A. M. Brabers, and R. Claessen, Europhys. Lett. **70,** 789 (2005).
[41] R. Aragón, P. M. Gehring, and S. M. Shapiro, Phys. Rev. Lett. **70,** 1635 (1993).
[42] A. Kozłowski, Z. Kąkol, D. Kim, R. Zalecki, and J. M. Honig, Phys. Rev. B **54,** 12 093 (1996).